Interaction of graphene nanoparticles and lipid membranes displaying different liquid ordering: a molecular dynamics study.

Elle Puigpelat[1], Jordi Ignés-Mullol[1], Francesc Sagués[1], Ramon Reigada[1,2,]*

[1] Department de Ciència dels Materials i Química Física and [2]Institut de Química Teòrica i Computacional (IQTCUB), Universitat de Barcelona, c/ Martí i Franqués 1, Pta 4, 08028 Barcelona Spain

ABSTRACT. Understanding the effects of graphene-based nanomaterials on lipid membranes is fundamental to determine their environmental impact and the efficiency of their biomedical use. By means of molecular dynamics simulations of simple model lipid bilayers, we analyse in detail the different interaction modes. We have studied bilayers consisting of lipid species (including cholesterol) which display different internal liquid ordering. Nanometric graphene layers can be transiently adsorbed onto the lipid membrane and/or inserted in its hydrophobic region. Once inserted, graphene nanometric flakes display a diffusive dynamics in the membrane plane, they adopt diverse orientations depending on their size and oxidation degree, and they show a particular aversion to be placed close to cholesterol molecules in the membrane. Addition

of graphene to phase-segregated ternary membranes is also investigated in the context of the lipid raft model for the lipid organization of biological membranes. Our simulation results show that graphene layers can be inserted indistinctly in the ordered and disordered regions. Once inserted, nanometric flakes migrate to disordered and cholesterol-poor lipid phases.

INTRODUCTION

Carbon-based nanomaterials have received extensive attention due to their unique properties.[1] In particular, graphene, which can be described as a single layer of carbon atoms arranged in a honeycomb lattice, exhibits peculiar and interesting properties due to its two-dimensional nature.[2-4] The interest in this material and its derivatives has exploded exponentially since 2004 when it was first synthetized and characterized.[5] Graphene oxide (GO), produced by oxidation of graphite under acidic conditions, is the graphene derivative most commonly used. GO offers several advantages over using pure graphene since it is dispersible in aqueous media, which is essential for many applications, and it has also broader ranges of physical properties than pure graphene due to its structural heterogeneity.[6]

In the last 15 years, many efforts have been devoted to explore potential applications of GO derivatives in the fields of biomedicine[7] and biotechnology.[8] Drugs, biomolecules, quantum dots, polymers and nanoparticles can be conjugated with graphene, and these graphene-based nano-composites can be used as drug delivery vehicles,[9] analytical and sensing devices,[10] antibacterial agents,[11] or they can be applied in cell imaging,[12] tissue engineering[13] and gene transfection.[14] However, despite the unquestionable advances achieved in this field, application of graphene nano-materials in biomedicine and biotechnology is still limited by the incomplete knowledge of

the fate of graphene-based nanoparticles in biological systems that may cause adverse side effects. Additionally, as production of graphene rapidly grows, a concern for its toxicity[15] and environmental impact[16] emerges as an issue that needs to be urgently addressed. Graphene has been reported to exhibit toxicity effects on bacteria[17] and human cell lines.[18] Other investigations have suggested that it may exert cytotoxicity via different modes of action including plasma membrane damage, impairment of mitochondrial function, induction of oxidative stress, apoptosis, and DNA damage.[18-20] The size of graphene nanoparticles falls into the category of potentially inhaled materials and, thus, it may enter the circulatory system and accumulate in different organs including liver, spleen and kidney.[21-22]

Summing up the concerns about possible side effects and toxicity, there is an urgent need to understand potential physiological and pathological reactions of biological systems to the exposure of graphene. In this regard, understanding the interaction of graphene nanoparticles with biologically relevant interfaces like the cell membrane is fundamental. From a methodological perspective, the use of *in vitro* and *in silico* strategies with simple lipid bilayer systems are extremely useful to approach more complex biological scenarios. For instance, a combined strategy using experimental and computational approaches has been recently used in a similar issue regarding the effect of Gold nanoparticles in biomimetic interfaces.[23]

Molecular dynamics (MD) simulations applied to simple and reproducible systems such as model lipid membranes provide an excellent approach to unveil the mechanisms of the interaction and gain insights on the physical principles governing them. Atomistic MD simulations, however, are limited to short time (a few hundred of ns) and length scales (10-20 nm). Consequently, we use a coarse-grained (CG) MD approach, which covers much longer scales while preserving the main molecular characteristics of the simulated moieties. The study

of the interaction between graphene and a lipid bilayer by means of CG MD simulations has been recently attempted using different approaches. These works are starting to provide insights on how graphene favorably interacts at the molecular level with lipid membranes through self-assembly of graphene nanosheets in lipid membranes[24] and membrane penetration of graphene.[25,26] Several experimental studies have also been successful at unveiling some of the characteristics of graphene-membrane interactions that may eventually lead to graphene absorption, bilayer disruption and other interaction modes,[27–32] including the formation of multilayered graphene/membrane structures, the generation of pores in vesicle membranes, the insertion of graphene into liposomes or the complete destruction of the bilayer configuration.[29-31]

In our contribution, we propose to apply MD simulations to analyze the interaction of graphene with cholesterol-containing membranes with a double objective. First, cholesterol (Chol) is a key compound present in all eukaryotic cell membranes that determines their structure, fluidity and permeability, so its specific interplay with graphene particles in a lipid bilayer deserves particular attention. Second, cholesterol has also an important role in determining how lipids and proteins are partitioned in biological membranes. It is well known that eukaryotic cell membranes are organized in domains rich in cholesterol and saturated lipids referred to as rafts, embedded in a medium mostly containing unsaturated lipids. Such structures are endowed with membrane protein sorting properties and, as a consequence, with many biological functions.[33,34] Although some aspects of the raft phenomenology still remain controversial, it is accepted that the coexistence of differently ordered liquid phases constitutes the thermodynamic basis for raft organization. Ternary synthetic lipid bilayers are able to reproduce the coexistence of liquid phases when saturated and unsaturated lipids become separated into a liquid-ordered (*lo*) phase and a liquid-disordered (*ld*) phase once cholesterol is

added to the membrane mixture. Summing up, it is fundamental that simulated membranes contain cholesterol and display lipid heterogeneity in the form of *lo*/*ld* coexistence in order to approach the complexity of biological membranes.

In our contribution, nanometric graphene flakes and lipid membranes formed by phospholipid moieties with different degrees of saturation and containing different fractions of cholesterol are considered. Size, oxidation degree and initial orientation of nanometric graphene layers are systematically varied to elucidate their role in the interaction with lipid membranes. As a result, different interaction modes have been observed (insertion and adsorption) and special attention is paid to the role of cholesterol and lipid ordering in the interaction behavior.

METHODS

Coarse-graining approach and simulated molecules. Our simulations follow the coarse-grained (CG) model proposed by the Martini v2.0 force field.[35] This model applies a 4-to-1 mapping and it has been successfully applied to study a large variety of lipid membrane phenomena,[36-38] including the interaction with carbon-based nanomaterials.[25,39] The numerical simulations are carried out for membranes consisting of three phosphatidylcholines (PC) displaying different levels of unsaturation in their acyl chains (see Fig. 1): DUPC (with two double-unsaturated linoleoyl 16:2 tails), POPC (with an unsaturated oleoyl 18:1 tail and a saturated palmitoyl 16:0 tail) and DPPC (with two saturated palmitoyl 16:0 tails). Each PC is described by a positively charged choline group, a negatively charged phosphate, two neutral glycerols, and two tails with four (for linoleoyl and palmitoyl tails) or five (for the oleoyl tails) apolar particle beads. Cholesterol is also added to the simulated membranes. Cholesterol

molecules are composed by eight particles: a polar bead for the hydroxyl group, five beads representing the ring sterol system and two beads for the short alkyl tail (see Fig. 1).

The CG parameterization of graphene and graphene oxide flakes follows the hexagonal lattice proposed in Ref. 40 that reproduces quite well many structural and mechanical graphene properties. The Martini force field recommends a 3-to-1 mapping for the description of molecules with rings but here we choose the 4-to-1 coarse-graining in order to preserve the original hexagonal lattice symmetry of graphene as it has been successfully used in previous simulations.[27,40,41] Other carbon-based nanomaterials like nanotubes[42] and fullerenes[39,43] have also been successfully modeled following a 4-to-1 approach.

Different graphene layers varying in size and oxidation degree are used in our simulations. Size will be described by the number of beads (*#beads*) forming the layer as G*#beads*; for instance, G54 is a graphene layer composed by 54 beads. Size is varied from small layers with a linear size smaller than membrane thickness (G54; 1.94 nm x 2.24 nm) to large layers with a linear size slightly larger than common membrane thickness (G350; 5.82 nm x 5.60 nm). The intermediate sizes are: G120 (3.395 nm x 3.08 nm) and G190 (4.365 nm x 3.92 nm). The oxidation degree is varied from 0% (all graphene beads are apolar) to 20% (one in five beads are randomly given a polar character).

Simulation protocols. The simulations are performed using the GROMACS v.4.5.5 software package[44] and they are carried out in the NpT ensemble through a weak coupling algorithm at T=310K and an anisotropic pressure p= 1 bar. Electrostatic interactions are handled using a shifted Coulombic potential energy form and charges are screened with a relative dielectric constant ε_r= 15. Periodic boundary conditions are used in all three directions, and the time step is set to 20 fs.

Simulated membrane-graphene systems. To evaluate the effect of cholesterol, two membranes have been first simulated: the first one is composed by 576 molecules of POPC and the second membrane is made of 576 POPC and 248 Chol (30 mol%) molecules. Both systems are conveniently hydrated with 16,000 water molecules, 12.5% of which are antifreeze waters.[35] A graphene layer is placed in the aqueous phase at a distance of ~1 nm of the equilibrated membrane. We vary the layer size and its oxidation degree, and for each case, different initial graphene orientations are considered by placing one of its faces, edges or corners proximal to the membrane. Additional simulations are performed starting from graphene-inserted configurations in order to observe the effects on graphene's accommodation inside the vesicle bilayer. All graphene/membrane systems are initially subjected to an energy minimization process in order to eliminate possible particle overlaps, and production runs of at least 1.2 μs are finally performed for all cases.

A ternary membrane system is initially built as a random mixture of the 828 DUPC molecules (42.6 mol%), 540 saturated DPPC molecules (27.8 mol%) and 576 Chol molecules (29.6 mol%), equally distributed in the two leaflets. The membrane is conveniently hydrated with 32,000 water molecules, energy minimization is performed and it is then equilibrated for 18 μs at T= 295K to allow complete phase separation. Visual inspection of the equilibration process reveals a clear phase segregation process for the two simulated ternary membranes: the saturated lipid forms a packed lipid phase (*lo*) together with Chol molecules, segregated from a disordered phase (*ld*) rich in the unsaturated lipid (DUPC). Equilibration is assured by tracking a segregation parameter that accounts for the average number of lateral neighbors of the same molecular kind (details in Ref. 38). The differences in the interaction between graphene and the two segregating phases are studied by approaching the corner of G120 layers (0 and 20% oxidized) to each lipid

phase and analyzing the corresponding insertion processes as well as the behavior of the graphene particles inserted in the heterogeneous membrane.

***Umbrella* sampling method**. The free energy profiles (potential of mean force, PMF) for a graphene flake traversing the simulated lipid bilayers are calculated using the *umbrella* sampling method.[45] Four types of smaller membranes are used for this purpose: a pure POPC bilayer formed by 200 POPC molecules, its cholesterol-containing counterpart formed by 144 POPC and 62 Chol molecules, a disordered *ld*-like membrane consisting of 200 DUPC molecules, and a ordered *ld*-like bilayer formed by 144 DPPC and 62 Chol molecules. The four bilayers are hydrated with 4,000 water particles. Once the membrane systems are equilibrated, the PMF(z) are calculated for a small G36 flake (0 or 20% oxidized) traversing the membrane in a length of 8 nm. Series of 50 independent simulation windows are conducted with the center of mass of graphene fixed by a harmonic constraint around positions in 0.16 nm steps. Each umbrella simulation window is conducted for 300 ns (200 ns of equilibration). The analysis of the *umbrella* simulations is performed using the weighted histogram analysis method (WHAM).[46]

RESULTS and DISCUSSION

Graphene-membrane interaction modes: insertion and adsorption

In our simulations, graphene nanosheets with different sizes and degrees of oxidation are approached (corner, edge or face proximal < 1 nm) to equilibrated POPC and POPC/Chol membranes. As a general behavior, nanometric graphene particles spontaneously translocate to the membrane due to its preference to be placed at the bilayer hydrophobic core. The driving force of graphene insertion is determined by the attractive interaction between graphene and the hydrophobic lipid acyl chains placed in the inner region of the membrane. As it is reported in

previous MD studies,[24-27] graphene penetration is preferentially started at corners or asperities; all simulated flakes that initially approach one of their edges or corners to the lipid bilayer spontaneously pierce the membrane, and due to the attractive interactions with lipid acyl chains, they are pulled inside towards the membrane apolar region until complete insertion (Fig. 2a). The penetration process is qualitatively similar regardless of the size and oxidation degree of the graphene particle, but its kinetics may vary. We find that oxidized particles penetrate more slowly than non-oxidized ones. For instance, the apolar G120 layer in Fig. 2a becomes completely inserted in the membrane in a fraction of a microsecond whereas its 20%-oxidized counterpart requires more than one microsecond to complete the same process (see Fig. 2b). On what respects to the graphene size, as expected, the smaller the graphene particle is, the shorter is the time required for its complete coverage within the membrane. As an example, Fig. 2c shows how a small non-oxidized G54 flake gets completely embedded in the membrane in approximately 80 ns. Interestingly, no significant differences are noticed when comparing the interaction with POPC and POPC/Chol bilayers; at this level of description the presence of cholesterol does not affect the general behavior.

When the approach of graphene to the membrane is attempted frontally, diverse situations have been observed. Most cases display a quick rotation of the graphene flake in the aqueous phase so that one of its corners or edges pierces the membrane and the insertion process takes place spontaneously, as in the case described in Fig. 2c. In some cases, however, the graphene layer first diffuses away from the bilayer and performs a random trajectory in the aqueous phase before contacting again the membrane surface by a corner or edge, and displays spontaneous penetration. Finally, a third scenario has been captured, in particular for oxidized and moderately large (G120 and larger) graphene particles that corresponds to their frontal adsorption on the

proximal bilayer leaflet. The details of this interaction mode are presented in Fig. 2d for a G120 oxidized sheet in a POPC/Chol membrane: the graphene is adsorbed and approaches the bilayer core by moving apart the polar headgroups of the contacting lipid leaflet, whose apolar chains are then twisted and arranged tangentially to the bilayer plane in order to offer a hydrophobic accommodation (Fig. 2d). As a result, the membrane becomes locally thinner and, interestingly, cholesterol molecules are found to avoid the contacting leaflet just below the adsorbed layer since they are much more rigid than PC moieties. Although the adsorption mode does not correspond to the minimum energy configuration for the graphene/membrane system, its lifetime seems to be longer than those achievable in CG MD simulations. For instance, the graphene layer in Fig. 2d remains adsorbed after a long 5 μs simulation. Transient adsorption of graphene layers on small liposome membranes has been already reported in recent CG MD studies.[27]

From a technical point of view, it is important to notice here that a few of the simulations working with the largest graphene layers (G350) result in artificial freezing of the surrounding aqueous phase. This happens in those circumstances when graphene does not quickly interact (insertion or adsorption) with the lipid membrane, and corresponds to a typical artifact appearing in CG MD when simulating the interaction of soft-matter systems with large solid (ordered) assemblies. Unfortunately, the use of antifreeze CG water particles cannot avoid this problem and this is the reason for not simulating larger graphene particles than G350 in our study. Previous simulations overcome this issue by covering graphene with the lipid membrane constituents.[25,26]

Membrane-inserted graphene layers: low affinity for cholesterol and orientation

The analysis of the behavior of inserted graphene flakes reveals a significant trend to avoid graphene/cholesterol contacts. We have computed the number of POPC and Chol molecules,

N_{POPC} and N_{Chol}, proximal to the inserted graphene particle. A lipid molecule is considered in contact with graphene when any of its constituent beads is closer than 0.5 nm to a graphene particle. The amount of proximal POPC molecules for G54, G120 and G190 particles (for 0 and 20% oxidation degree) is of the order of 13, 23 and 30, respectively, whereas in all cases N_{Chol} oscillates around one single proximal cholesterol molecule. The relative amount N_{POPC}/N_{Chol} is therefore about 4 to 10 times higher than the POPC/Chol ratio in the simulated bilayer. The depletion of Chol molecules around graphene flakes can be attributed to their mutual non-conformability and other entropic considerations.[27] Once the graphene layer adopts the perpendicular configuration it undergoes fast Brownian motion, including "lateral" diffusion along the membrane and rapid rotation. All these motion modes are more favoured when graphene is surrounded with flexible PC molecules than when it is close to rigid cholesterol particles.

The presence of cholesterol also affects other aspects of graphene behavior once inserted in the membrane. For instance, our simulated G54, G120 and G190 graphene sheets display a perpendicular orientation respect to the membrane plane. The orientation angle, α, computed as the angle between the normal vector of the graphene plane and the (x,y) plane of the membrane, oscillates around a very low value. The averaged value of α for graphene inserted in the POPC/Chol membrane is in the range 3º-8º depending on the flake size and oxidation degree. Although still rather perpendicular, graphene sheets are allowed to be a little bit more tilted (10º-15º) when inserted in a pure POPC bilayer. Lipid condensation and packing produced by cholesterol are likely to be responsible for such effect. As a consequence of this ordering ability, cholesterol also reduces the lateral mobility of inserted graphene. Diffusive motion is observed in the plane of the membrane for all perpendicularly inserted G54, G120 and G190 particles.

Estimations of graphene diffusion coefficients lie in the range of 4-7.5x10^{-8} $cm^2 \cdot s^{-1}$ when inserted in POPC membranes, whereas the mobility is reduced to 2.7-3.8x10^{-8} $cm^2 \cdot s^{-1}$ in the POPC/Chol membrane. The diffusivity of POPC molecules in a pure lipid membrane is higher than the corresponding to larger graphene particles (D_{POPC}=17x10^{-8} $cm^2 \cdot s^{-1}$), and a reduction due to the presence of 30 mol% of cholesterol is also observed (D_{POPC}=8.0x10^{-8} $cm^2 \cdot s^{-1}$).

Previous studies based on CG MD simulations of simple graphene/membrane systems reported that inserted graphene sheets generally adopt a parallel arrangement at the mid-plane of the membrane,[24,25] although some results indicate that a perpendicular, or at least tilted, conformation has to be considered as well.[26,27] More specifically, atomistic simulations have recently demonstrated that small graphene sheets prefer to adopt a perpendicular orientation respect to the membrane plane; namely, parallel to lipid molecules.[47] All graphene particles that end up embedded in the membrane in our simulations adopt this latter configuration. In order to check whether this conformation is the most stable or a transient state, we have conducted simulations with the graphene flakes initially lying flat in the bilayer center. Interestingly, all the smallest particles (G54), regardless their oxidation degree or the characteristics of the hosting membrane (POPC or POPC/Chol), rotate from the initial horizontal position to a vertical orientation (see Fig. 3a). In all cases the orientation angle α is initially close to 90º with slight fluctuations for a period of time until a strong fluctuation triggers the rotation motion that it is completed rather quickly in few nanoseconds (Fig. 3b). In all cases, the remaining trajectory (up to 4.5 μs) of graphene sheets preserves the vertical orientation with α fluctuating at low values. It is important to notice from Fig. 3b that graphene rotation takes place sooner (i.e. more easily) when the lipid environment is less packed (pure POPC membrane) since larger orientation fluctuations are allowed in these membranes than in more ordered ones (POPC/Chol system).

Additionally, oxidized graphene particles rotate sooner than nonpolar ones as a consequence of the extra stabilization achieved by the perpendicular orientation due to favorable contacts between water and polar regions of graphene.

The stability of the vertical orientation is confirmed by looking at the interaction energy among system components, and in particular those involving graphene. In Fig. 3c the total interaction potential energy of graphene respect to the other system components, E_G, is plotted for 20%-oxidized G54 sheets placed either vertically in a POPC/Chol membrane or lying flat between the membrane leaflets. The rotation observed in the latter case allows graphene to be about 70 $kJ \cdot mol^{-1}$ more stable (Fig. 3c). Most of the stabilization is due to a significant increase of POPC-graphene contacts when graphene adopts the perpendicular orientation.

The discrepancy with the results reported so far from CG simulations[24-26] can be attributed to the size of the simulated graphene layers that are significantly larger than the ones considered here. Although the vertical orientation is energetically favoured for G120 and G190 (not shown), rotation is not observed after 4.8 μs of simulations when they are placed lying flat between membranes layers. A representative example is found in Fig. 3b for a 20%-oxidized G120 sandwiched in a POPC membrane (the most favorable situation for rotation). Notice that in this case, angle fluctuations are reduced compared with smaller graphene particles, and this is likely to be the reason to explain why rotation is not observed and graphene remains trapped in the horizontal metastable configuration.

The vertical orientation of inserted graphene nanosheets has an important impact on the lipid tail alignment of surrounding PC molecules. The ordering of lipid chains can be characterized by the order parameter $S_{tail} = \frac{1}{2}(3\,cos^2\theta - 1)$, where θ is the angle between the normal of the membrane plane and the vector between bonded acyl lipid beads. The order parameter ranges

from complete alignment (S_{tail}=1) to a random orientation (S_{tail}=0) We have computed S_{tail} by averaging all lipid tails over 400 ns of simulation for POPC membranes with and without inserted graphene. In the case of the membrane containing a G120 non-oxidized graphene the order parameter is calculated for neighboring POPC molecules (at least one bead at a distance closer than 1 nm to a graphene particle), and for distant POPC molecules (all their forming beads farther than 2 nm to the graphene flake). The ordering effect of graphene on membrane lipids is clear and significant for neighboring POPC molecules where we obtain S_{tail}= 0.46, while we get S_{tail}= 0.35 for distant POPC molecules. The order parameter for POPC molecules in a graphene-free membrane displays the same value than the one obtained for distant POPC molecules in the membrane containing graphene, indicating that the ordering effect is local and only affects the PC molecules in direct contact with the inserted graphene particle.

Graphene insertion into different lipid-ordered bilayers: the raft approach

Membrane lipid composition and internal ordering regulate the interaction between the bilayer system and graphene nanoparticles. First, we analyze how these factors affect graphene insertion by computing the free energy profiles (potential of mean force, PMF) for graphene particles as a function of their distance to the bilayer center of mass. Unfortunately, the *umbrella* sampling procedure fails when using the graphene particles simulated so far in our simulations due to the strong membrane deformations generated when graphene is placed close the membrane/water interphase. This problem is overcome with the use of smaller G36 nanolayers (1,40 nm x 1,70 nm) that do not damage the bilayer structure during the *umbrella* procedure. Four different systems are studied; the POPC and POPC/Chol bilayers analyzed so far in previous sections, and two extremely disordered and ordered systems such as DUPC and DPPC/Chol membranes, mimicking the *ld* and *lo* lipid phases appearing in heterogeneous membranes, respectively.

The PMF profiles for 0% and 20%-oxidized graphene particles traversing the four membrane systems are plotted in Figure 4 together with the corresponding transversal lipid density profiles. Some common features for all analyzed systems can be noted. First, inappreciable penetration barriers are obtained, in agreement with previous estimations.[25,26] Second, strong graphene stabilization is obtained inside the hydrophobic membrane core, in a range from 40 to 80 k_BT (25-50 kcal·mol^{-1}) with respect to water (where the PMF is taken as zero). Third, as expected, stabilization is significantly (30-35%) reduced for oxidized graphene particles.

The differences observed among the four analyzed bilayers can be explained by understanding the energy profiles as a balance between two opposing effects: the cost of vacating the space to be occupied by graphene, and the dispersion interactions resulting from inserting the graphene particle into the vacancy.[48] The first aspect strongly depends on the flexibility and adaptability of the membrane constituent species, whereas the second contribution is maximized at the densest lipid environments. Interestingly, cholesterol contributes to the two opposite effects: we already reported the non-favorable interactions of Chol with graphene, but it makes the bilayers more compact due to its condensation action. By comparing the POPC and POPC/Chol cases, deeper energy minima are obtained in the absence of cholesterol. For nonpolar flakes energy minima of -46.9 and -41.5 kcal·mol^{-1} are obtained in the absence and in the presence of cholesterol, respectively. For 20%-oxidized graphene, the energy stabilization is reduced and more pronounced again in the absence than in presence of cholesterol (-33.0 and -28.6 kcal·mol^{-1}, respectively). The non-favorable effect of cholesterol, therefore, dominates. In both membrane systems, the energy minima are found around 1 nm, the densest regions of the membrane that are usually located immediately below the glycerol backbone. For the POPC/Chol system the energy

minimum is displaced a little bit farther towards the bilayer center since cholesterol thickens the membrane (at 1.1 nm respect to 0.9 nm in the absence of cholesterol).

The membrane composed of the more disordered lipid (DUPC, formed by four unsaturated tail beads that occupy most of the hydrophobic membrane region) displays stabilization energies of -43.3 and -27.8 kcal·mol^{-1} for 0 and 20%-oxidized layers, respectively. Those values are a little bit smaller than for the POPC membrane since the DUPC system has a lower lipid density. Notice that the energy minima are displaced to the DUPC bilayer center (at 0.4-0.6 nm), that corresponds to the highest density region of this membrane system. For the DPPC/Chol membrane energy stabilization is reduced (-40.4 and -26.3 kcal·mol^{-1} for 0 and 20%-oxidized layers, respectively). The energy minima are placed at 1 nm of distance to the bilayer midplane, coinciding with the densest region of the DPPC/Chol membrane. Comparing the two extreme ordered/disordered lipid systems, the PMF calculation reveals that the presence of cholesterol reduces the stability of inserted graphene particles in the *lo*-like membrane respect to the bilayer resembling the *ld* phase. The non-favourable interaction between graphene and cholesterol reported previously seems to dominate respect to the increase of the number of dispersion interactions due to the cholesterol condensation effect.

Some of the conclusions discussed so far can be reinforced by analyzing the dynamic behavior of graphene flakes inserted into a membrane displaying *lo*/*ld* coexistence (see Fig. 5). We use an equilibrated DUPC/DPPC/Chol membrane that displays phase-segregation of a raft-like *lo* domain with molar composition 0.05/0.49/0.46 from a *ld* phase with composition 0.84/0.1/0.06. The *lo* phase occupies a 42% of the total membrane area, and the segregated phases are transversally aligned in the two leaflets. We approach (~1 nm) the corner of individual G120 layers (0 and 20% oxidized) to each lipid phase and analyze their insertion and their dynamic

behavior inside the heterogeneous membrane. We have attempted 10 different initial graphene approaching locations to each liquid phase, and in all cases the insertion takes place rather immediately. Insertion in the ordered phase is a little bit slower than in the disordered phase, but preserving the insertion time scales reported so far. As it has been discussed previously, 20% oxidized particles display a slower insertion kinetics, but no significant influence of the hosting lipid phase is observed either. In agreement with the absence of a penetration energy barrier in all the computed PMF profiles, graphene is equally able to enter a raft-like membrane by its ordered or disordered domains. In Supplementary Information Figure S1, experiments show that graphene particles get adsorbed on simple vesicle membranes and how graphene adhesion on heterogeneous vesicles does not indicate any preference of graphene particles to be inserted in the *lo* or *ld* phases.

In order to analyze the behavior of the inserted graphene particles we extend up to 18 μs four simulations for the raft membrane (one for each graphene oxidation degree being inserted in each one of the lipid phases). In all cases the graphene layers remain inserted and perpendicular to the bilayer, and display Brownian motion in the membrane plane. Interestingly and in accordance with PMF calculations, graphene flakes that are initially placed in a *lo* environment progressively migrate to the *ld* phase (Fig. 5a). We quantify the *lo*/*ld* degree of graphene lipid environment by computing the Δ parameter as $\Delta = \frac{N_{DUPC} - N_{DPPC} - N_{Chol}}{N_{DUPC} + N_{DPPC} + N_{Chol}}$ where N_i corresponds to the number of lipid molecules *i* that are proximal to graphene. For a graphene sheet fully placed in the *ld* (*lo*) phase, the value of Δ is equal to +1 (-1). We observe that in all cases Δ tends to +1, even when graphene is initially inserted in a *lo* domain. As an example, in Fig. 5b we plot the temporal evolution of Δ (that turns from negative values to +1 in several microseconds) and the number of contacting lipid molecules for the trajectory in Fig. 5a, demonstrating the preference of inserted

graphene nanolayers to migrate to the *ld* lipid environment as a consequence of its nonfavourable interaction with cholesterol molecules (see the inset in Fig. 5b).

CONCLUSIONS

By means of a collection of coarse-grained MD simulations, we analyse the interaction between graphene and simple lipid bilayers as a simplified model of the cell membrane, the first barrier that graphene encounters when contacting a biological system. Studying this interaction provides a starting point to understand the cytotoxicity of graphene and/or its efficiency in biomedical applications. Our MD simulations confirmed the affinity of graphene for the inner hydrophobic region of a lipid membrane. Graphene penetration is spontaneous and preferentially started at corners or asperities, with similar features regardless of the size and oxidation degree of the graphene particle, although its kinetics may vary: oxidized and larger sheets penetrate more slowly than apolar and smaller ones. We have also reported an interaction mode where the graphene sheet is adsorbed on the headgroup region of one of the leaflets of the membrane by moving apart the polar headgroups and contacting the inner hydrophobic bilayer core. This adsorption mode is preferentially obtained for our simulated large and oxidized graphene sheets frontally approaching the membrane.

Simulations show that lipid bilayers are good solvents for nano-sized (of the order of the membrane thickness or smaller) graphene flakes that, once inserted, adopt a rather perpendicular orientation respect to the membrane plane; namely, parallel to lipid molecules, in contrast to the results reported in previous studies based on CG MD simulations. The combination of simulations with the graphene flakes initially lying flat in the bilayer center or placed perpendicular to the membrane demonstrates that the latter is the most favorable configuration.

Interestingly, a detailed analysis of the behavior of graphene flakes inserted in Chol-containing membranes reveals a significant trend to avoid graphene/cholesterol contacts that can be explained by their mutual molecular non-conformability. Lateral lipid packing produced by cholesterol is responsible of two additional effects. First, although nano-sized graphene sheets display a perpendicular orientation, they are allowed to perform tilt variations more pronouncedly when inserted in bilayers without cholesterol. Second, cholesterol significantly reduces the lateral mobility of inserted graphene nanosheets. No previous results on the detailed interaction with cholesterol has been reported in the literature despite the relevance of this compound in biological membranes.

Due to the relevance of raft formation in biological membranes, the behavior of graphene in differently ordered lipid phases, and in heterogeneous membranes displaying *lo*/*ld* coexistence has been analyzed. Simulations show how graphene enters the bilayer indistinctly and spontaneously through ordered or disordered regions. Once inserted, nano-sized graphene particles are allowed to diffuse along the membrane and display a preference to migrate to the disordered (*ld*) phases where cholesterol is less abundant. This conclusion is of important relevance since the preference of graphene nanoparticles to be dissolved in the more disordered regions of a lipid bilayer may have important consequences on the activity in biological cell membranes and on the bioconcentration of graphene in living organisms.

AUTHOR INFORMATION

Corresponding Author

*E-mail for correspondence: reigada@ub.edu

Notes

The authors declare no competing financial interest.

ACKNOWLEDGMENTS

The authors acknowledge financial support from the Spanish Ministry of Economy and Competitiveness (MINECO) through project FIS2016-78507-C2-1-P.

ABBREVIATIONS

GO, graphene oxide; MD, molecular dynamics; CG, coarse-grained; POPC, 1-Palmitoyl-2-oleoyl-phosphatidylcholine; DPPC, 1,2-dipalmitoyl-phosphatidylcholine; DOPC, 1,2-dioleoyl-phosphatidylcholine; DUPC, 1,2-dilinoleoyl-phosphatidylcholine; Chol, cholesterol; *lo*, liquid-ordered; *ld*, liquid-disordered; PMF, potential of mean force.

SUPPORTING INFORMATION

Experimental set up for vesicle formation and observation of graphene-vesicle interactions (Supporting Text); Vesicle electroformation cell (Figure S1); Adsorption of graphene in heterogeneous lipid vesicles (Figure S2)

REFERENCES

(1) Cha, C.; Shin, S. R.; Annabi, N.; Dokmeci, M. R.; Khademhosseini, A. Carbon-Based Nanomaterials: Multifunctional Materials for Biomedical Engineering. *ACS Nano* **2013**, *7* (4), 2891–2897.

(2) Castro Neto, A. H.; Guinea, F.; Peres, N. M. R.; Novoselov, K. S.; Geim, A. K. The Electronic Properties of Graphene. *Rev. Mod. Phys.* **2009**, *81* (1), 109–162.

(3) Geim, A. K.; Novoselov, K. S. The Rise of Graphene. *Nat. Mater.* **2007**, *6* (3), 183–191.

(4) Chen, D.; Tang, L.; Li, J. Graphene-Based Materials in Electrochemistry. *Chem. Soc. Rev.* **2010**, *39* (8), 3157–3180.

(5) Novoselov, K. S.; Geim, A. K.; Morozov, S. V.; Jiang, D.; Zhang, Y.; Dubonos, S. V.; Grigorieva, I. V.; Firsov, A. A. Electric field effect in atomically thin carbon films. *Science* **2004**, 306, 666-669.

(6) Dreyer, D. R.; Park, S.; Bielawski, W.; Ruoff, R. S. The Chemistry of Graphene Oxide. *Chem. Soc. Rev.* **2010**, *39*, 228-240.

(7) Yang, K.; Feng, L.; Shi, X.; Liu Z. Nano-graphene in biomedicine: theranostic applications. *Chem. Soc. Rev.* **2013**, *42*, 530-547.

(8) Singh, D. P.; Herrera C. E.; Singh, B.; Singh, S.; Singh, R. K.; Kumar, R. Graphene oxide: an efficient material and recent approach for biotechnological and biomedical applications. *Mater. Sci. Eng. C* **2018**, *86*, 173-197.

(9) Liu, Z.; Robinson, J. T.; Sun, X.; Dai, H. PEGylated Nanographene Oxide for Delivery of Water-Insoluble Cancer Drugs. *J. Am. Chem. Soc.* **2008**, 10876–10877.

(10) Liu, Y.; Dong, X.; Chen, P. Biological and Chemical Sensors Based on Graphene Materials. *Chem. Soc. Rev.* **2012**, *41* (6), 2283–2307.

(11) Yuan, H.; Huang, C.; Li, J.; Lykotrafitis, G.; Zhang, S. One-Particle-Thick, Solvent-Free, Coarse-Grained Model for Biological and Biomimetic Fluid Membranes. *Phys. Rev. E - Stat. Nonlinear, Soft Matter Phys.* **2010**, *82* (1), 1–8.

(12) Sun, X.; Liu, Z.; Welsher, K.; Robinson, J. T.; Goodwin, A.; Zaric, S.; Dai, H. Nano-Graphene Oxide for Cellular Imaging and Drug Delivery. *Nano Res.* **2008**, *1* (3), 203–212.

(13) Sayyar, S.; Murray, E.; Thompson, B. C.; Gambhir, S.; Officer, D. L.; Wallace, G. G. Covalently Linked Biocompatible Graphene/Polycaprolactone Composites for Tissue Engineering. *Carbon* **2013**, *52*, 296–304.

(14) Feng, L.; Zhang, S.; Liu, Z. Graphene based gene transfection. *Nanoscale* **2011**, *3*, 1252-1257.

(15) Seabra, A. B.; Paula, A. J.; De Lima, R.; Alves, O. L.; Durán, N. Nanotoxicity of Graphene and Graphene Oxide. *Chem. Res. Toxicol.* **2014**, *27* (2), 159–168.

(16) Sanchez, V. C.; Pietruska, J. R.; Miselis, N. R.; Hurt, H.; Kane, A. B. Biopersistence and Potential Adverse Health Impacts of Fibrous Nanomaterials: What Have We Learned from Asbestos?. *Wiley Interdiscip. Rev. Nanomed. Nanobiotechnol.* **2009**, *1(5)*, 511-529.

(17) Akhavan, O.; Ghaderi, E. Toxicity of Graphene and Graphene Oxide Nanowalls against Bacteria. *ACS Nano* **2010**, *4* (10), 5731–5736.

(18) Liao, K. H.; Lin, Y. S.; MacOsko, C. W.; Haynes, C. L. Cytotoxicity of Graphene Oxide and Graphene in Human Erythrocytes and Skin Fibroblasts. *ACS Appl. Mater. Interfaces* **2011**, *3* (7), 2607–2615.

(19) Akhavan, O.; Ghaderi, E.; Akhavan, A. Size-Dependent Genotoxicity of Graphene Nanoplatelets in Human Stem Cells. *Biomaterials* **2012**, *33* (32), 8017–8025.

(20) Li, Y.; Liu, Y.; Fu, Y.; Wei, T.; Le Guyader, L.; Gao, G.; Liu, R.-S.; Chang, Y.-Z.; Chen, C. The Triggering of Apoptosis in Macrophages by Pristine Graphene through the MAPK and TGF-Beta Signaling Pathways. *Biomaterials* **2012**, *33* (2), 402–411.

(21) Schinwald, A.; Murphy, F. A.; Jones, A.; MacNee, W.; Donaldson, K. Graphene-Based Nanoplatelets: A New Risk to the Respiratory System as a Consequence of Their Unusual Aerodynamic Properties. *ACS Nano* **2012**, *6* (1), 736–746.

(22) Wang, Y.; Aker, W. G.; Hwang, H.; Yedjou, C. G.; Yu, H.; Tchounwou, P. B. A Study of the Mechanism of in Vitro Cytotoxicity of Metal Oxide Nanoparticles Using Catfish Primary Hepatocytes and Human HepG2 Cells. *Sci. Total Environ.* **2011**, *409* (22), 4753–4762.

(23) Pfeiffer, T.; De Nicola, A.; Montis, C.; Carlà, F.; van der Vegt, N. F. A.; Berti, D.; Milano, G. Nanoparticles at biomimetic interfaces: combined experimental and simulation study on charged Gold nanoparticles/lipid bilayer interfaces. *J. Phys. Chem. Lett.* **2019**, *10*, 129-137

(24) Titov, A. V; Kra, P.; Pearson, R. Sandwiched Graphene-Membrane Superstructures. *ACS Nano* **2010**, *4* (1), 229–234.

(25) Wang, J.; Wei, Y.; Shi, X.; Gao, H. Cellular entry of graphene nanosheets: the role of thickness, oxidation and surface adsorption. *RSC Advances* **2013**, *3*, 15776–15782.

(26) Li, Y.; Yuan, H.; von dem Bussche, A.; Creighton, M.; Hurt, R. H.; Kane, A. B.; Gao, H. Graphene Microsheets Enter Cells through Spontaneous Membrane Penetration at Edge Asperities and Corner Sites. *Proc. Natl. Acad. Sci.* **2013**, *110* (30), 12295–12300.

(27) Santiago, R.; Reigada, R. Interaction modes between nanosized graphene flakes and liposomes: Adsorption, insertion and membrane fusion. *Biochim. et Biophys. Acta General Subjects* 2019, *1863*, 723-731.

(28) Rui, L.; Liu, J.; Li, J.; Weng, Y.; Dou, Y.; Yuan, B.; Yang, K.; Ma, Y. Reduced Graphene Oxide Directed Self-Assembly of Phospholipid Monolayers in Liquid and Gel Phases. *Biochim. Biophys. Acta - Biomembr.* **2015**, *1848 (5)*, 1203-1211.

(29) Huang, P. J. J.; Wang, F.; Liu, J. Liposome/Graphene Oxide Interaction Studied by Isothermal Titration Calorimetry. *Langmuir* **2016**, *32* (10), 2458–2463.

(30) Liu, X.; Chen, K. L. Interactions of Graphene Oxide with Model Cell Membranes: Probing Nanoparticle Attachment and Lipid Bilayer Disruption. *Langmuir* **2015**, *31* (44), 12076-12086.

(31) Frost, R.; Svedhem, S.; Langhammer, C.; Kasemo, B. Graphene Oxide and Lipid Membranes: Size-Dependent Interactions. *Langmuir* **2016**, *32* (11), 2708–2717.

(32) Wu, L.; Zeng, L.; Jiang, X. Revealing the Nature of Interaction between Graphene Oxide and Lipid Membrane by Surface-Enhanced Infrared Absorption Spectroscopy. *J. Am. Chem. Soc.* **2015**, *137* (32), 10052–10055.

(33) Simons, K.; Ikonen, E. Functional rafts in cell membranes. *Nature* **1997**, *387*, 569-572.

(34) Simons, K.; Toomre, D. Lipid rafts and signal transduction. *Nat. Rev. Mol. Cell Biol.* **2000**, *1*, 31-39.

(35) Marrink, S. J.; Risselada, H. J.; Yefimov, S.; Tieleman, D. P.; de Vries, A. H. The MARTINI Force Field: Coarse Grained Model for Biomolecular Simulations. *J. Phys. Chem. B* **2007**, *111*, 7812–7824.

(36) Marrink, S. J.; Tieleman, D. P. Perspective on the Martini Model. *Chem. Soc. Rev.* **2013**, *42* (16), 6801–6822.

(37) Mannelli, I.; Sagués, F.; Pruneri, V.; Reigada, R. Lipid Vesicle Interaction with Hydrophobic Surfaces: A Coarse-Grained Molecular Dynamics Study. *Langmuir* **2016**, *32* (48), 12632–12640.

(38) Reigada, R.; Sagués, F. Chloroform Alters Interleaflet Interaction in Lipid Bilayers: An Entropic Mechanism. J. R. Soc. Interface **2015**, *12*, 20150197.

(39) Sastre, J.; Mannelli, I.; Reigada, R. Effects of Fullerene on Lipid Bilayers Displaying Different Liquid Ordering: A Coarse-Grained Molecular Dynamics Study. *Biochim. Biophys. Acta - Gen. Subj.* **2017**, *1861* (11), 2872–2882.

(40) Ruiz, L.; Xia, W.; Meng, Z.; Keten, S. A Coarse-Grained Model for the Mechanical Behavior of Multi-Layer Graphene. *Carbon* **2015**, *82*, 103–115.

(41) Wu, D.; Yang, X. Coarse-Grained Molecular Simulation of Self-Assembly for Nonionic Surfactants on Graphene Nanostructures. *J. Phys. Chem. B* **2012**, *116* (39), 12048–12056.

(42) Wallace, E. J.; Sansom, M. S. P. Carbon Nanotube/Detergent Interactions via Coarse-Grained Molecular Dynamics. *Nano Lett*. **2007**, *7* (7), 1923–1928.

(43) Wong-Ekkabut, J.; Baoukina, S.; Triampo, W.; Tang, I.-M.; Tieleman, D. P.; Monticelli, L. Computer Simulation Study of Fullerene Translocation through Lipid Membranes. *Nat. Nanotechnol*. **2008**, *3*, 363-368.

(44) Lindahl, E.; Hess, B.; van der Spoel, D. GROMACS 3.0: A Package for Molecular Simulation and Trajectory Analysis. *Mol. Model. Annu*. **2001**, *7* (8), 306–317.

(45) Torrie, G. M.; Valleau, J. P. Nonphysical Sampling Distributions in Monte Carlo Free-Energy Estimation: Umbrella Sampling. *J. Comput. Phys*. **1977**, *23* (2), 187–199.

(46) Hub, J. S.; Groot, B. L.; Spoel, D. G_wham—A Free Weighted Histogram Analysis Implementation Including Robust Error and Autocorrelation Estimates. *J. Chem. Theory Comput*. **2010**, *6*, 3713–3720.

(47) Chen, J.; Zhou, G.; Chen, L.; Wang, Y.; Wang, X.; Zeng, S. Interaction of graphene and its oxide with lipid membrane: a molecular dynamics simulation study. *J. Phys. Chem. C* **2016**, 120, 6225-6231.

(48) Marrink, S. J.; Berendsen, H. J. C. Permeations process of small molecules across lipid membranes studied by molecular dynamics simulations. *J. Phys. Chem*. **1996**, 100, 16729-16738.

FIGURES

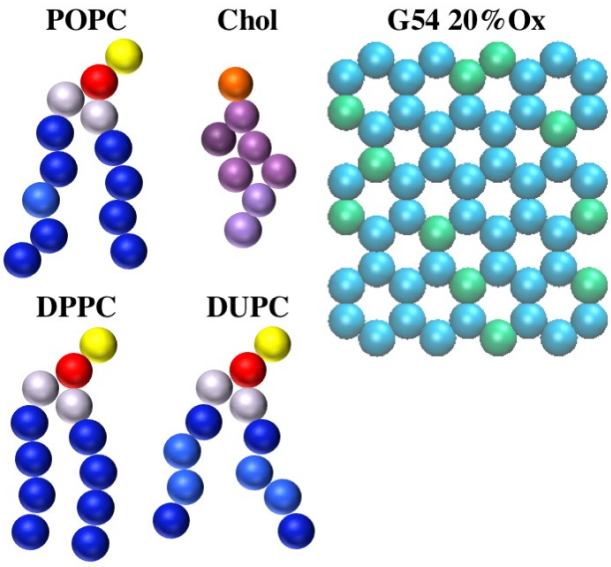

Figure 1. Schematic CG Martini representation of the simulated molecules. Blue beads correspond to apolar particles forming the PC tails (dark: unsaturated segments, light: saturated segments) and violet is used for Chol apolar beads (dark: ring structure, light: saturated ending tail). Red, yellow, white and orange beads stand for choline, phosphate, glycerol and hydroxyl groups, respectively. A representation of a G54 graphene oxide flake is also provided, with apolar carbon beads in cyan and 20% of oxidized (polar) groups in green.

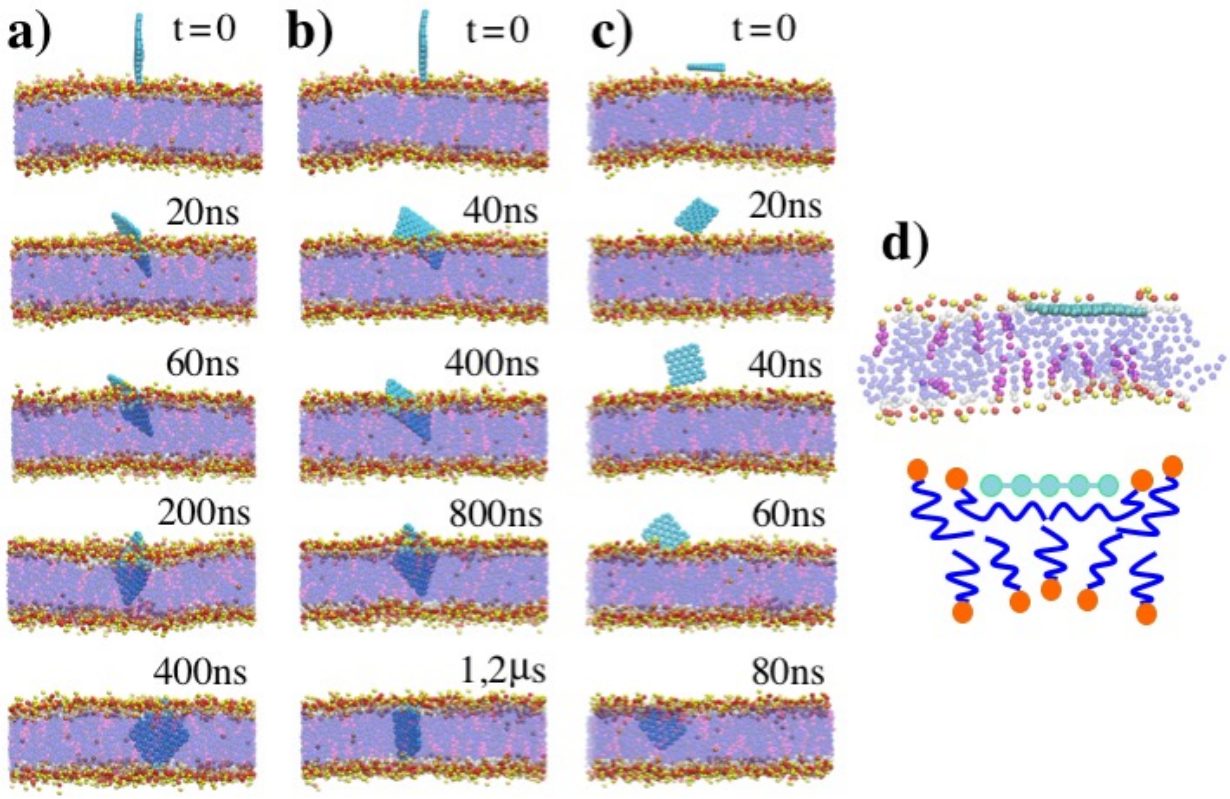

Figure 2. Temporal sequence of the insertion of a non-oxidized (a) and a 20%-oxidized (b) G120 graphene layer in a POPC/Chol membrane. In both cases one corner of the graphene sheet is initially placed proximal to the bilayer. Non-oxidized graphene penetrates faster the membrane than the oxidized one. In panel (c), a small G54 flake quickly pierces a POPC/Chol bilayer by one of its corners although it is initially placed with a frontal orientation. In panel (d) the detail of the configuration of lipid molecules close to an adsorbed oxidized G120 layer is shown, together with a schematic representation of how lipid molecules (orange and blue) accommodate the graphene particle (cyan). The color code for the molecular representation is the same as in Fig.1a. Water particles are not plotted for clarity.

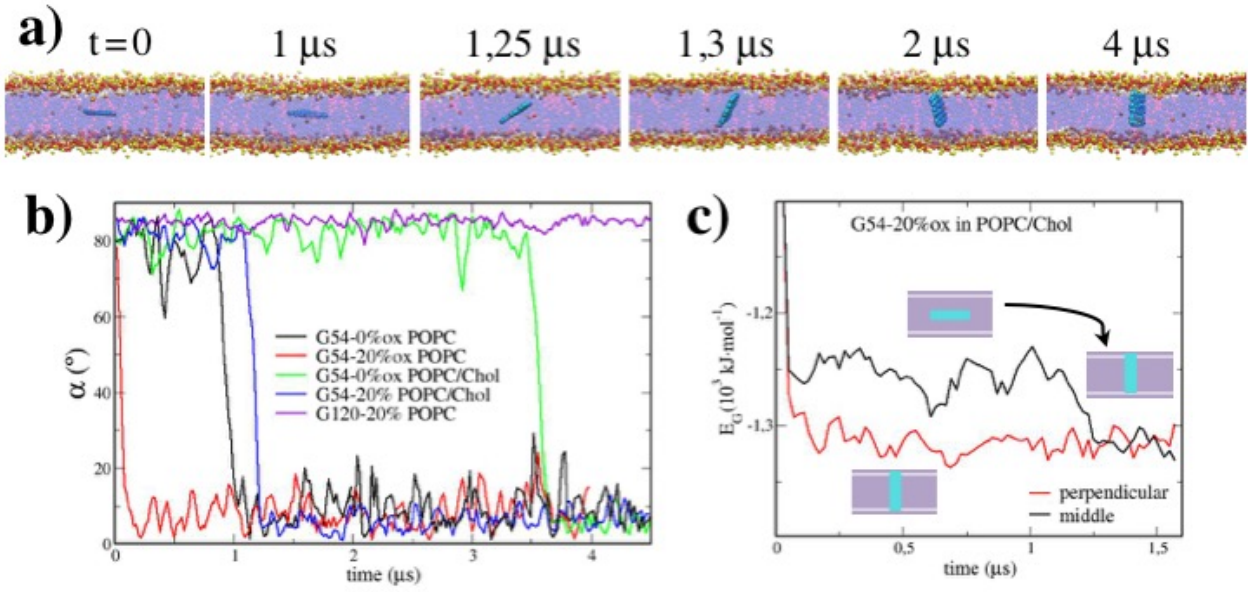

Figure 3. (a) Temporal sequence for a 20%-oxidized G54 layer initially sandwiched between the leaflets of a POPC/Chol membrane. The color code for the molecular representation is the same as in Figs.1a and 2. (b) Temporal evolution of the graphene orientation angle, α, for different G54 particles displaying rotation to a perpendicular orientation. A representative case for a G120 sheet that preserves the horizontal orientation is also plotted. (c) Total nonbonding potential energy for 20%-oxidized G54 particles that are initially placed in a horizontal or a perpendicular orientation inside a POPC/Chol membrane.

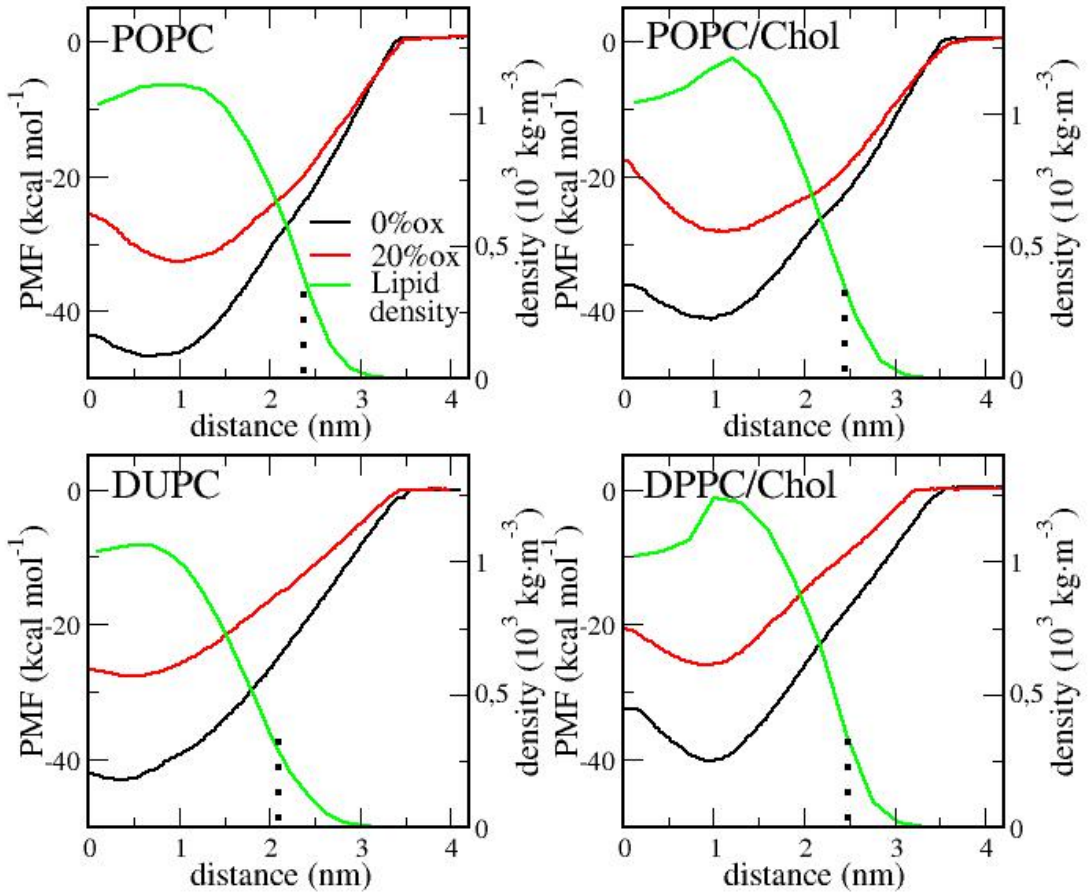

Figure 4. Energy profiles for graphene insertion. Potential of Mean Force (PMF) profiles are plotted for 0% and 20% oxidized G36 graphene particles (black and red, respectively) as a function of the distance respect to the membrane center. Four lipid bilayers displaying different composition and level of lipid ordering are analyzed. The right axis is used to represent the lipid density profile (green) for each membrane system. The vertical dotted lines indicate the average position of phosphate groups of PC molecules in the membrane.

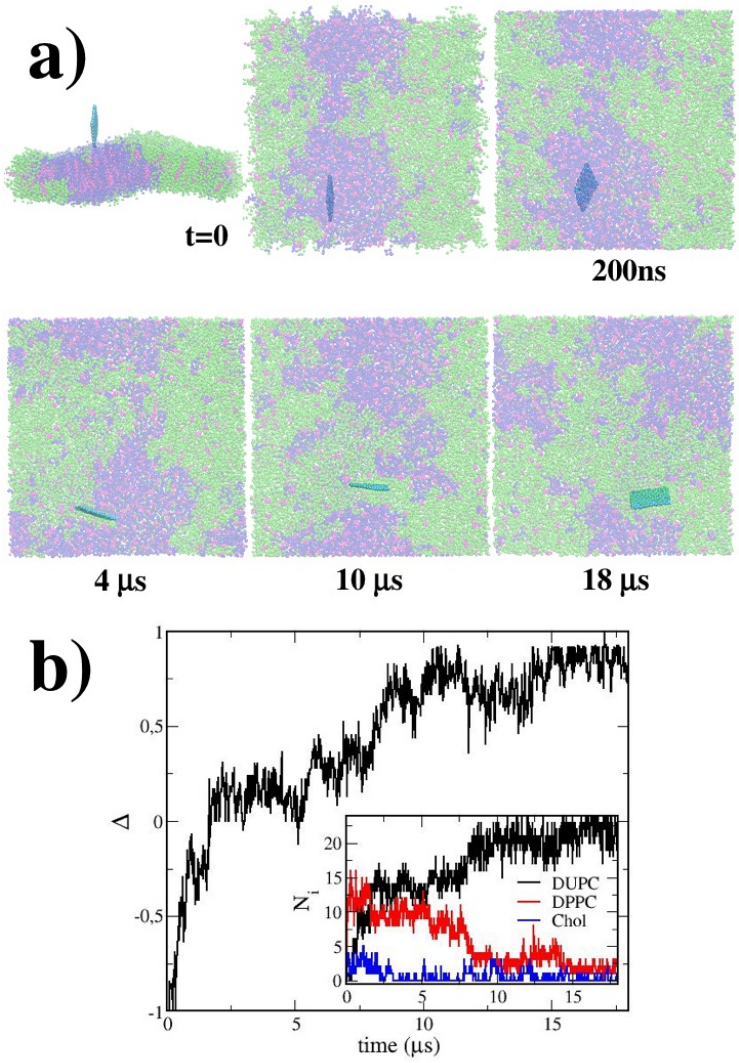

Figure 5. (a) Temporal sequence for the dynamics of a nonpolar graphene G120 particle (cyan) inserted in the *lo* domain. The liquid-ordered phase is rich in DPPC (blue) and cholesterol (violet), whereas the disordered phase is basically formed by DUPC (here in green; the color code is changed in order to visualize the two coexisting phases). Graphene escapes from the ordered domain and prefers to be placed in a disordered environment. (b) Temporal evolution of the Δ variable accounting for the *lo*/*ld* degree of the graphene surroundings for the case in panel (a). Inset: number of the different lipid species in close contact to the graphene particle.

TOC FIGURE

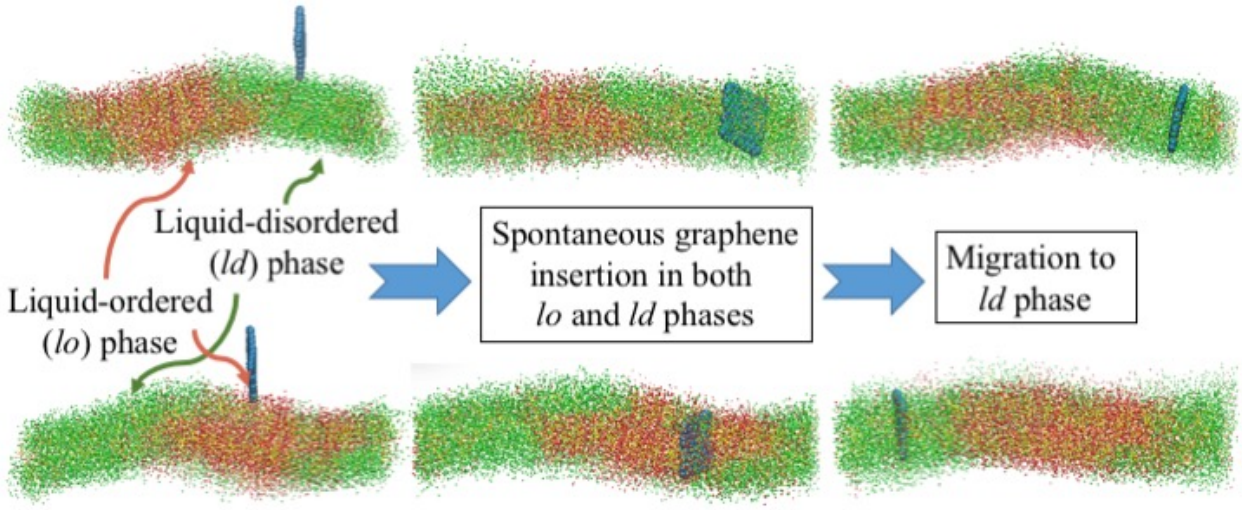
Liquid-disordered
(*ld*) phase
Liquid-ordered
(*lo*) phase
Spontaneous graphene
insertion in both
lo and *ld* phases
Migration to
ld phase